PNAS
www.pnas.org

Supplementary Information for
Modeling Links Softening of Myelin and Spectrin Scaffolds of Axons after a Concussion to Increased Vulnerability to Repeated Injuries

Aayush Kant, Victoria E. Johnson, John D. Arena, Jean-Pierre Dollé, Douglas H. Smith, Vivek B. Shenoy

* Vivek B. Shenoy
Email: vshenoy@seas.upenn.edu

This PDF file includes:

Supplementary text
Table S1
Figures S1 to S6
SI References

S.1 Extended Methods: Derivation of Rescaled Governing Equations

Considering the unit cell of length $2L$, as shown in Fig 2d, we begin by deriving the force-equilibrium equation for an infinitesimal section of a microtubule MT_i under the influence of microtubules MT_{i-1} above and MT_{i-1} below. Following the free body diagram in Fig 2e, the elongation of MT_i due to the transfer of load from the tissue to the MT lattice is $u_i(x,t)$. The deformation of cross-linkers between MT_i and MT_{i+1} can, therefore, be approximated as $\delta_\tau^{i,i+1} \approx u_{i+1}(x,t) - u_i(x,t)$. As discussed in Section 2.1, the force F_τ - deformation δ_τ relationship for the cross-linker is given as,

$$F_\tau = K_\tau\{\eta_\tau\dot{\delta}_\tau + \delta_\tau\} \tag{S1}$$

where the dot represents a time derivative. Similarly, the deformation of spectraplakin between the cortex and MT_1 is $\delta_{sp} \approx u_1(x,t) - u_s(x,t)$, where u_s is the elongation of the axonal cortex. The force F_{sp} - deformation δ_{sp} relationship for the cross-linker is given as $F_{sp} = K_{sp}\{\eta_{sp}\dot{\delta}_{sp} + \delta_{sp}\}$. A balance of forces in the axial direction over an infinitesimal region of the cortex and the microtubules MT_1, MT_2 and MT_3 gives the equations governing the stress in the cortex and the MTs as,

$$\begin{aligned} A_s\frac{\partial\sigma_s}{\partial x} &= -\frac{F_{sp}cos\beta_{sp}}{d_{sp}} \\ A_M\frac{\partial\sigma_1}{\partial x} &= \frac{F_{sp}cos\beta}{d_{sp}} - \frac{F_\tau^{1,2}\cos\beta_\tau}{d_\tau} \\ A_M\frac{\partial\sigma_2}{\partial x} &= \frac{F_\tau^{1,2}\cos\beta_\tau}{d_\tau} - \frac{F_\tau^{2,3}cos\beta_\tau}{d_\tau} \\ A_M\frac{\partial\sigma_3}{\partial x} &= \frac{F_\tau^{2,3}cos\beta_\tau}{d_\tau} - \frac{F_\tau^{3,4}cos\beta_\tau}{d_\tau} \end{aligned} \tag{S2}$$

Using Eq. (S1), the force transferred via the cross-linker between MT_i and MT_{i+1} is given as $F_\tau^{i,i+1} = K_\tau\{\eta_\tau(\dot{u}_{i+1} - \dot{u}_i) + (u_{i+1} - u_i)\}$. Assuming a linear elastic behavior for the MTs, the stress in MT_i can be written in terms of its elongation as, $\sigma_i = E_M\partial u_i/\partial x$. Substituting for these expressions in Eq. (S2), we get the equation governing the elongation of MT_i as,

$$2L_c^2\frac{\partial^2 u_i}{\partial x^2} + \eta_\tau(\dot{u}_{i+1} - 2\dot{u}_i + \dot{u}_{i-1}) + (u_{i+1} - 2u_i + u_{i-1}) = 0 \tag{S3}$$

where, $L_c = \sqrt{\left(\frac{A_M E_M d_\tau}{2*K_\tau cos\beta}\right)}$ is the characteristic length of load transfer for the microtubules [1]. For typical values of the parameters, listed in Table S1, $L_c = 8.76\,\mu$m. In Eq. (S3) the spatial and temporal coordinates can be rescaled as $X = x/L$ and $T = \dot{\sigma}t/\sigma_{max}$, where σ_{max} is a scaling constant, which denotes the maximum stress applied to the axonal cortex during the ramped loading. The displacement field thus rescales as $U_i(X,T) = u_i(x,t)/L$. This rescaling gives the modified force balance relation for microtubule MT_i as,

$$\frac{2L_c^2}{L^2}\frac{\partial^2 U_i}{\partial X^2} + \frac{\dot{\sigma}\eta_\tau}{\sigma_{max}}\left(\dot{U}_{i+1} - 2\dot{U}_i + \dot{U}_{i-1}\right) + (U_{i+1} - 2U_i + U_{i-1}) = 0 \tag{S3a}$$

It must be noted that for MT_1, we have the myelin-cortex bilayer on the top connected via spectraplakin cross-linker instead of tau. While writing Eq. (S3) and Eq. (S3a) for MT_1, we can incorporate this by replacing F_τ by F_{sp}. Since the spectraplakin may be connected at an angle β_{sp} distinct from β_τ, we will have additional coefficients in terms of $cos\,\beta_{sp}/\cos\,\beta_\tau$ in the velocity and deformation terms of Eq. (S3) and Eq. (S3a). Over here, as a general simplifying assumption, we

take $\beta_\tau = \beta_{sp} = \beta$. With these considerations, we can obtain the general governing equations for the cortical displacement field $U_s(X,T)$ and the three MT displacement fields, $U_i(X,T)(\text{for } i = 1,2,3)$ from Eq. (S3a) as,

$$
\begin{aligned}
2\left[\frac{\mathrm{A_s}}{\mathrm{A_M}}\frac{\mathrm{E_s}}{\mathrm{E_M}}\frac{\mathrm{d_{sp}}}{\mathrm{d_\tau}}\frac{\mathrm{K_\tau}}{\mathrm{K_{sp}}}\right]\frac{\mathrm{L_c^2}}{\mathrm{L^2}}\frac{\partial^2 \mathrm{U_s}}{\partial \mathrm{X^2}} + \frac{\dot{\sigma}\eta_\tau}{\sigma_{\max}}\frac{\eta_{sp}}{\eta_\tau}\left(\dot{\mathrm{U}}_1 - \dot{\mathrm{U}}_s\right) + (\mathrm{U}_1 - \mathrm{U_s}) = 0,\\
\frac{2\mathrm{L_c^2}}{\mathrm{L^2}}\frac{\partial^2 \mathrm{U}_1}{\partial \mathrm{X^2}} + \frac{\dot{\sigma}\eta_\tau}{\sigma_{\max}}\left[\dot{U}_2 - \left(\frac{\mathrm{K_{sp}/K_\tau}}{\mathrm{d_{sp}/d_\tau}}\frac{\eta_{sp}}{\eta_\tau} + 1\right)\dot{\mathrm{U}}_1 + \frac{\mathrm{K_{sp}/K_\tau}}{\mathrm{d_{sp}/d_\tau}}\frac{\eta_{sp}}{\eta_\tau}\dot{\mathrm{U}}_s\right]\\
+\left(\mathrm{U}_2 - \left(\frac{\mathrm{K_{sp}/K_\tau}}{\mathrm{d_{sp}/d_\tau}} + 1\right)\mathrm{U}_1 + \frac{\mathrm{K_{sp}/K_\tau}}{\mathrm{d_{sp}/d_\tau}}\mathrm{U_s}\right) = 0, \qquad (S4)\\
\frac{2\mathrm{L_c^2}}{\mathrm{L^2}}\frac{\partial^2 \mathrm{U}_2}{\partial \mathrm{X^2}} + \frac{\dot{\sigma}\eta_\tau}{\sigma_{\max}}\left(\dot{U}_3 - 2\dot{\mathrm{U}}_2 + \dot{\mathrm{U}}_1\right) + (\mathrm{U}_3 - 2\mathrm{U}_2 + \mathrm{U}_1) = 0, \qquad \text{and}\\
\frac{2\mathrm{L_c^2}}{\mathrm{L^2}}\frac{\partial^2 \mathrm{U}_3}{\partial \mathrm{X^2}} + 2\frac{\dot{\sigma}\eta_\tau}{\sigma_{\max}}\left(\dot{U}_2 - \dot{\mathrm{U}}_3\right) + 2(\mathrm{U}_2 - \mathrm{U}_3) = 0.
\end{aligned}
$$

The first of these equations applies to the myelin-cortex bilayer, while the next three to the microtubules MT_1, MT_2, and MT_3, respectively. We further note that many of the salient parameters arrange themselves into non-dimensional ratios listed in Table S1, which can be varied to account for parametric perturbations. Finally, the loading rate $\dot{\sigma}$ is normalized in Eq. (S4) as $\dot{\sigma}\eta_\tau/\sigma_{\max}$. Equations (S4) form the set of governing equations to be solved numerically to obtain the spatio-temporal evolution of stresses and strains in the cytoskeletal system.

Considering the horizontal symmetry of the unit cell shown in Fig 2d, and to accommodate the staggered MT arrangement, alternate MTs are fixed at their mid-points such that, $u_s(0,t) = 0$, $u_1(0,t) = 0$, and $u_3(0,T) = 0$. It has been shown by Krieg et al. [9] that extra-neuronal mechanical forces from the tissue are sensed by a neuron via the spectrin in the axonal cortex, suggesting that in an axon, the tissue stress is transmitted from the tissue to the intra-axonal cytoskeleton via the axonal cortex. Therefore, we apply a ramped tissue stress with a constant rate of $\dot{\sigma}$ to the myelin-cortex bilayer such that $E_s\frac{\partial u_s(L,t)}{\partial x} = \dot{\sigma}t$. The boundary and loading conditions can also be rescaled as $U_s(0,T) = 0,\ U_1(0,T) = 0,\ U_3(0,T) = 0$, and $\left.\frac{\partial U_s}{\partial X}\right|_{\mathrm{X=1}} = \frac{\sigma_{\max}\mathrm{T}}{\mathrm{E_s}}$. We solve Eq. (S4) along with the rescaled boundary and loading conditions numerically using the finite element package COMSOL 5.5.

Table S1: Values of Parameters used in the model

Parameter	Description	Value	Reference
E_M	MT elastic modulus	1.9 GPa	[5]
A_M	MT cross-sectional area	336.94 nm^2	[5]
K_τ	Tau protein spring constant	0.25 pN/nm	[1]
η_τ	Tau protein viscous parameter	0.35 s	[1]
d_τ	Tau protein spacing	30 nm	[1]
L_c	MT load transfer length scale	8.76 μm	(calculated)
Non-dimensional ratios in the rescaled model			
L/L_c	Non-dimensional MT half length	0.1	[6]
A_s/A_M	Relative cortical cross-sectional area	0.2	Approximated [7, 5]
d_{sp}/d_τ	Relative spectraplakin spacing	4	(Parametric study carried out for these parameters)
E_s/E_M	Relative cortical elasticity	0.01	
K_{sp}/K_τ	Relative spectraplakin stiffness	0.5	
η_{sp}/η_τ	Relative spectraplakin viscosity	0.25	

DAIs are often associated with neurofilament (NF) network compaction due to secondary chemical degradations via phosphorylation or proteolysis, resulting in alterations in their axonal transport and axon caliber management functions [2, 3]. However, the contribution of NFs to the architectural properties of axon and its sustainability under mechanical loading is expected to be negligible [4]. Hence, we have not considered them in the present model. Since a TBI occurs in the form of short duration rotational and translational kinematic impulses translated through brain tissue, regions of tissue experience a spatially variable local mechanical stress. Due to the anisotropic nature of brain tissue, the local tissue stress translates into dynamic axial loads along the fiber tracts of the axons.

S.2 Extended Methods: Decoupling axonal cortex and myelin

In the previous section, and in the main manuscript, we have assumed that the myelin and the axonal cortex are tightly coupled to each other – such that they are considered to be a single elastic bilayer. This is motivated by the understanding from the literature that the myelin is wrapped tightly around the axolemma, such that there is no slip permitted between the two.

In this section of the SI, we shall relax this assumption. We now consider myelin and cortex to be independent layers (Fig S1a), with independent model parameters – areas of cross-section (A_m and A_s respectively) and elastic moduli (E_m and E_s respectively). In addition to these new parameters, we must now consider the mechanism of load transfer from the myelin sheath to the axonal cortex. Cytoskeletal proteins such as myelin-associated glycoproteins (MAGs) have previously been implicated in the axon-myelin interactions [8]. As with other cross-linkers in our model, we can consider these to be as a sequence of spring-dashpots – following a rate-dependent viscoelastic behavior – distributed with a separation of d_m. The mechanical properties of these proteins (stiffness K_m and viscosity η_m) govern the coupling between myelin and the cortex. For instance, we would expect that as K_m grows, myelin and cortex are more tightly coupled, as in the model in the main manuscript.

Consider the new schematic showing the transfer of dynamic mechanical forces from the tissue to the MTs via the myelin and cortex, as shown in Fig S1b. As previously, the balance of axial forces in each of the elastic layers gives the following five governing equations:

$$\begin{aligned}
A_m \frac{\partial \sigma_m}{\partial x} &= -\frac{F_m cos\beta_m}{d_m} \\
A_s \frac{\partial \sigma_s}{\partial x} &= \frac{F_m cos\beta_m}{d_m} - \frac{F_{sp} cos\beta_{sp}}{d_{sp}} \\
A_M \frac{\partial \sigma_1}{\partial x} &= \frac{F_{sp} cos\beta}{d_{sp}} - \frac{F_\tau^{1,2} \cos\beta_\tau}{d_\tau} \\
A_M \frac{\partial \sigma_2}{\partial x} &= \frac{F_\tau^{1,2} \cos\beta_\tau}{d_\tau} - \frac{F_\tau^{2,3} cos\beta_\tau}{d_\tau} \\
A_M \frac{\partial \sigma_3}{\partial x} &= \frac{F_\tau^{2,3} cos\beta_\tau}{d_\tau} - \frac{F_\tau^{3,4} cos\beta_\tau}{d_\tau}
\end{aligned} \qquad (S5)$$

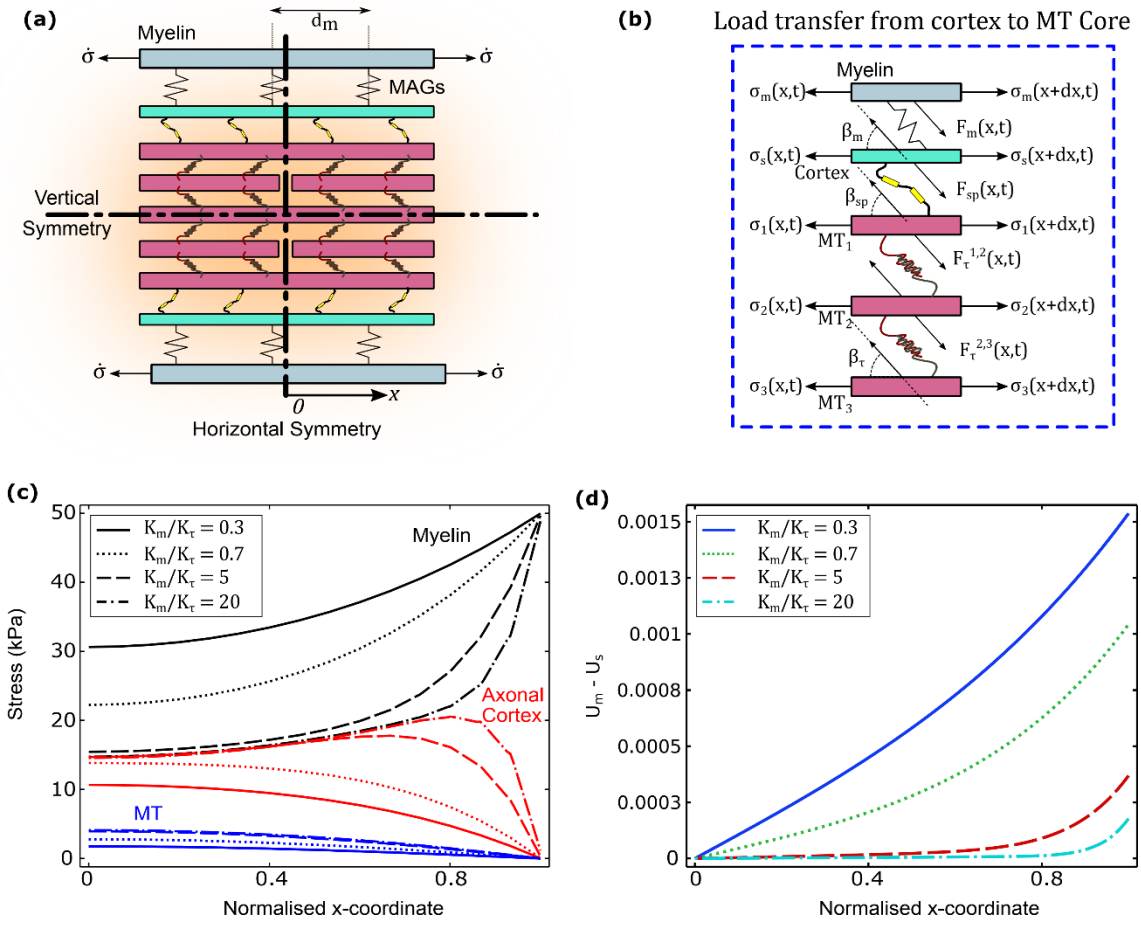

Fig S1: *The modified model – with decoupled myelin and axonal cortex. (a) A schematic showing an additional elastic layer of myelin over the cortex and MTs in an axon. The myelin is interlinked with the axonal cortex via the myelin associated glycoproteins (MAGs). (b) A schematic showing the transfer of stress from the tissue via the myelin and the axonal cortex to the MTs. (c) The stress in the myelin (black curves), the axonal cortex (red) and the outermost MT (blue) as the tissue stresses are transferred to the axon under different values of MAG stiffness (relative to that of tau proteins). (d) The normalized relative deformation* $(U_m - U_s)$ *between the myelin and the axonal cortex under different values of MAG stiffness. As the MAG stiffness increases, the stresses and deformation in the myelin and cortex become similar – allowing us to couple them into a single bilayer in our model.*

As previously, substituting the elastic relations for the axial stresses σ_i and the forces across the cross-linkers F_i, and normalizing the variables we get the governing equations for the model as,

$$2\left[\frac{\mathbf{A_m}}{\mathbf{A_M}}\frac{\mathbf{E}_{\boldsymbol{m}}}{\mathbf{E_M}}\frac{\mathbf{d_m}}{\mathbf{d_\tau}}\frac{\mathbf{K_\tau}}{\mathbf{K_m}}\right]\frac{L_c^2}{L^2}\frac{\partial^2 U_m}{\partial X^2}+\frac{\dot{\sigma}\eta_\tau}{\sigma_{max}}\frac{\boldsymbol{\eta_m}}{\boldsymbol{\eta_\tau}}\left(\dot{U}_s-\dot{U}_m\right)+\left(U_s-U_m\right)=0,$$

$$2\left[\frac{A_s}{A_M}\frac{E_s}{E_M}\right]\frac{L_c^2}{L^2}\frac{\partial^2 U_s}{\partial X^2}+\frac{\dot{\sigma}\eta_\tau}{\sigma_{max}}\left[\frac{K_{sp}/K_\tau}{d_{sp}/d_\tau}\frac{\eta_{sp}}{\eta_\tau}\dot{U}_1-\left(\frac{K_{sp}/K_\tau}{d_{sp}/d_\tau}\frac{\eta_{sp}}{\eta_\tau}+\frac{\mathbf{K_m/K_\tau}}{\mathbf{d_m/d_\tau}}\frac{\boldsymbol{\eta_m}}{\boldsymbol{\eta_\tau}}\right)\dot{U}_s+\frac{\mathbf{K_m/K_\tau}}{\mathbf{d_m/d_\tau}}\frac{\boldsymbol{\eta_m}}{\boldsymbol{\eta_\tau}}\dot{U}_m\right]+$$
$$\left[\frac{K_{sp}/K_\tau}{d_{sp}/d_\tau}U_1-\left(\frac{K_{sp}/K_\tau}{d_{sp}/d_\tau}+\frac{\mathbf{K_m/K_\tau}}{\mathbf{d_m/d_\tau}}\right)U_s+\frac{\mathbf{K_m/K_\tau}}{\mathbf{d_m/d_\tau}}U_m\right]=0,$$

$$\frac{2L_c^2}{L^2}\frac{\partial^2 U_1}{\partial X^2}+\frac{\dot{\sigma}\eta_\tau}{\sigma_{max}}\left[\dot{U}_2-\left(\frac{K_{sp}/K_\tau}{d_{sp}/d_\tau}\frac{\eta_{sp}}{\eta_\tau}+1\right)\dot{U}_1+\frac{K_{sp}/K_\tau}{d_{sp}/d_\tau}\frac{\eta_{sp}}{\eta_\tau}\dot{U}_s\right]+ \qquad (S6)$$
$$\left(U_2-\left(\frac{K_{sp}/K_\tau}{d_{sp}/d_\tau}+1\right)U_1+\frac{K_{sp}/K_\tau}{d_{sp}/d_\tau}U_s\right)=0,$$

$$\frac{2L_c^2}{L^2}\frac{\partial^2 U_2}{\partial X^2}+\frac{\dot{\sigma}\eta_\tau}{\sigma_{max}}\left(\dot{U}_3-2\dot{U}_2+\dot{U}_1\right)+\left(U_3-2U_2+U_1\right)=0, \qquad \text{and}$$

$$\frac{2L_c^2}{L^2}\frac{\partial^2 U_3}{\partial X^2}+2\frac{\dot{\sigma}\eta_\tau}{\sigma_{max}}\left(\dot{U}_2-\dot{U}_3\right)+2\left(U_2-U_3\right)=0.$$

The first of these equations applies to the myelin, the second to the cortex, and the next three to the first, second and the third MTs (refer Fig S1b). As previously, accounting for the horizontal symmetry of the unit cell along with staggered arrangement of MTs, we use the displacement constraints, $U_m(0,t)=0,\ U_s(0,t)=0,\ U_1(0,t)=0$, and $U_3(0,T)=0$. The tissue load is applied on the myelin layer (Fig S1a) in a ramped fashion as $E_m\frac{\partial u_m(L,t)}{\partial x}=\dot{\sigma}t$.

In order to show the effect of the strength of coupling numerically, we vary the magnitude of relative MAG stiffness (K_m/K_τ) and observe the load transfer from the tissues to the MT. In Fig S1c we show the stress developed in the myelin sheath, the axonal cortex and MT1 as K_m/K_τ increases from 0.3 to 20. In Fig S1d the difference in the elongation of myelin and the axonal cortex (U_m-U_s) is shown for the same set of parameters. It can clearly be seen that as K_m/K_τ increases the myelin sheath and the axonal cortex behave like a single layer (same stress and elongation) validating our assertion that under a fully coupled scenario, as is physiologically relevant, we can couple them into a single bilayer.

There are a few points of interest we would like to note here:

(i) By adding a new layer to the model, we have ended up adding **five** new parameters shown in Eq. (S6) in bold font.

(ii) Addition of a new layer does not change the governing equations for the MTs (comparing the last three equations in Eq. (S4) and Eq. (S6)),

(iii) Lastly, and most importantly, if the myelin and cortex are fully coupled by making the relative MAG stiffness infinite ($K_m/K_\tau\to\infty$),

   a. the first equation in Eq. (S6) identically reduces to $U_s=U_m$ and $\dot{U}_s=\dot{U}_m$, which implies that myelin and cortex elongate together (as assumed in the fully coupled model), and,

   b. the following four equations in Eq. (S6) become equivalent to the four equations previously derived in Eq. (S4).

Thus, we would like to assert that under the conditions of full coupling between the myelin and axonal cortex this model is exactly the same as the model we follow in our manuscript. Under

physiological normal conditions, prior to occurrence of any injury, myelin is tightly wrapped around the axon disallowing any slip between the two [9]. However, we definitely agree that this model present a few advantages over the coupled model we follow:

(i) Having decoupled myelin and cortex, we can now study their degradation independently. These degradations may follow different timescales, thus allowing us to identify pathologies of either myelin (e.g. MBP loss) or spectrin (SNTF) in the cortex which would affect the axon more significantly.

(ii) This model could be further developed to allow capturing a few demyelination pathologies such as decompaction of myelin or separation of myelin from the axon.

In this section of the SI we have proposed a new model by uncoupling the myelin and the axonal cortex. We have additionally shown the effect of this coupling via a parametric study and confirmed that under the assumption of tight coupling (as is appropriate for an axon) the model reduces to the myelin-cortex bilayer model we propose in the main manuscript. If accurate values of the additional parameters are made available via experiments, the advantages of this model would overcome the current limitations.

S.3 Rotational Acceleration Model of Mild TBI

All experiments were conducted in accordance with protocols approved by The University of Pennsylvania Institutional Animal Care and Use Committee. Under general anesthesia, 6-month old female Hanford miniature swine underwent the rotational acceleration model of TBI, which induces injury via forces caused by rotational acceleration/deceleration due to pure impulsive centroidal head rotation [10, 11, 12, 13]. The size of the brain is critical with respect to the resultant pathology in TBI, as mass effects between regions of tissue can create high strains during dynamic brain deformation and rapid accelerations [14, 15]. Accordingly, injury parameters in this model were scaled relative to brain mass to generate mechanical loading of brain tissue relevant to human TBI.

Animals underwent 1. repetitive rotational injuries performed 24 hours apart with survival of 72 hours from the first injury (n=3); 2. single rotational injury with survival of 48 hours (n=2) or 72 hours (n=3) as previously reported [12] (selected to match the survival duration from both exposures in the repetitive group) and 3. shams (n=3).

Briefly, following induction of anesthesia using 0.4 mg/kg midazolam IM and 5% inhaled isoflurane, animals were intubated, and anesthesia maintained using 2.5% inhaled isoflurane. The HYGE pneumatic actuator device was used to induce pure impulsive centroidal head rotation of up to $110°$ in the coronal plane with a peak angular velocity of 225-248 rad/sec. The HYGE actuator generates linear motion via the triggered release of pressurized nitrogen which is then converted to angular motion via a custom-designed linkage assembly to induce rotation over ~20ms. Rotational kinematics were recorded using angular velocity transducers (Applied Technology Associates) mounted to the linkage sidearm coupled to a National Instruments data acquisition system running custom LabView software (10 kHz sampling rate). Notably, there is an absence of any head impact or forces arising from linear acceleration or deceleration. The level of rotation was selected based on previous clinical and neuropathological characterization that demonstrated findings consistent with mild TBI. Specifically, rapid mobilization occurs (within 5-10 minutes) following withdrawal of isoflurane, indicating an absence of prolonged loss of consciousness. In addition, no focal neurological deficits or altered mental status are observed acutely post-injury and prior neuropathological characterization demonstrates an absence of the complex pathologies of severe TBI including hemorrhagic lesions, ischemia or brain swelling [12, 13]. All aspects of the experiment were conducted in sham animals absent the rotation.

Animals were recovered from anesthesia and returned to the housing facility. While the procedure is non-surgical, preemptive analgesia was provided post-injury in the form of 0.1-3 mg of Buprenex (slow release preparation) SQ and acetaminophen 50 mg/kg PR.

At the study endpoint, all animals were deeply anesthetized and transcardially perfused using chilled heparinized saline followed by 10% neutral buffered formalin (NBF). Brains were subsequently post-fixed for 7 days in 10% NBF, sectioned into 5 mm blocks in the coronal plane and processed to paraffin using standard techniques.

S.4 Role of model parameters in load transfer mechanism

Longer MTs experience higher stress

A geometrical parameter, the microtubule length, is also expected to affect the load transfer mechanics. It has been reported that neurons experiencing greater stresses in-vivo tend to have shorter MTs [16]. Also, neurons with long MTs when mutated to be spectrin-deficient, are found to display significantly shorter MTs [16]. These results suggest that the extent of transfer of tissue stress to the MT bundle plays a vital role in limiting the length of MTs. Our group has previously shown that longer microtubules experience higher stresses for the same loading conditions and hence fail more readily [1]. From the mathematical modeling approach in Hossein et al. [1], it is expected that for shorter MTs, the load transfer occurs due to the elongation of cross-linkers resulting in sliding of MTs over each other. As the MT length increases and approaches the characteristic length L_c, the MTs start stretching rather than sliding, resulting in a higher MT strain and thus MT stress. Indeed, upon decreasing the normalized MT half- length $\left(\frac{L}{L_c}\right)$ from 0.1 to 0.08, we observed a reduced load transfer to the MTs, resulting in a 22.5% decrease in the MT stress (from 6.41 kPa to 4.97 kPa). On the other hand, increasing the normalized MT half- length $\left(\frac{L}{L_c}\right)$ from 0.1 to 0.2 resulted in a 25.3% increase in the MT stress (from 6.41 kPa to 8.03 kPa). Thus, axons containing longer MTs are more susceptible to mechanical damage. The susceptibility of such axons is further increased due to increased load transfer after neurochemical damage during secondary injuries.

Softer and more sparsely distributed spectraplakin reduce the load transfer to the MTs

From the myelin-cortex bilayer, the loads from the tissue stresses are transferred to the spectraplakin cross-linkers. Thus, the spectraplakin constitutive parameters – relative spectraplakin stiffness $\left(K_{sp}/K_{\tau}\right)$, and relative spectraplakin viscosity $\left(\eta_{sp}/\eta_{\tau}\right)$ must play a considerable role in the transfer of tissue stress to MT core. Here, we use the model to predict the MT stress at three values of relative spectraplakin stiffness $\left(K_{sp}/K_{\tau}\right)$ - 0.25, 0.5, and 1 keeping all other parameters unchanged. Figure S2 shows the spatial variation of stress in the cortex and MTs over the non-dimensional length of the half-unit cell. As the spectraplakin become stiff, load transferred $\left(= k_{sp}(u_s - u_1)\right)$from the cortex to the MTs increases. As a result, with increasing spectraplakin stiffness, the stress in the MT increases while that in the axonal cortex reduces, as shown in insets (1) and (2). Therefore, an increase in the spectraplakin stiffness is detrimental to microtubules, increasing the vulnerability of MT lattice to DAI. Further, stiffer spectraplakin linkers arrest the cortical elongation u_s more effectively, increasing the apparent stiffness of the axon. Schematics in insets (1) and (2) of Fig S2 show the variation in cortical elongation as the spectraplakin stiffness increases.

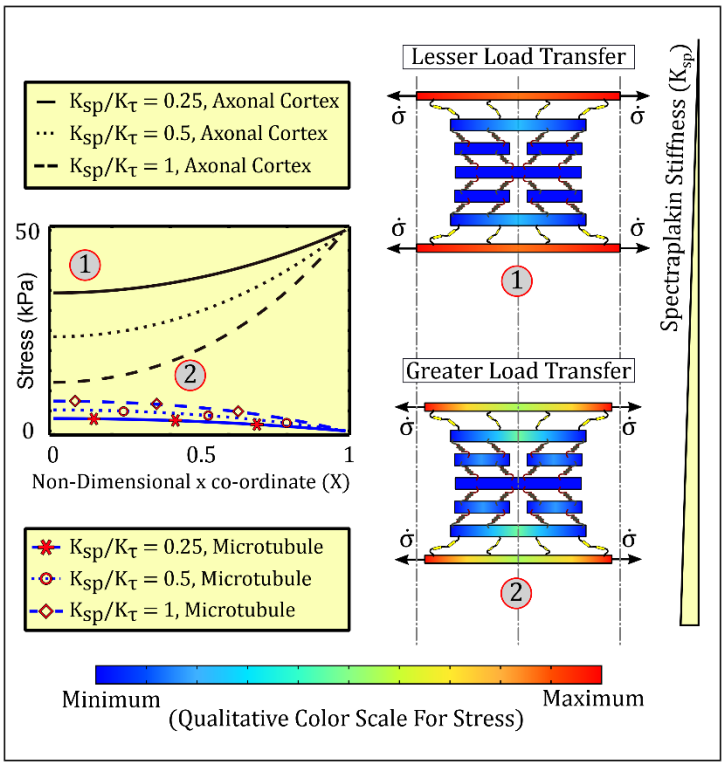

Fig S2: *The effect of model parameter spectraplakin stiffness on the spatial variation in the spectrin (black, no markers) and microtubule (blue, with red markers) stress over the length of the half unit cell. (a) As the non-dimensional spectraplakin stiffness* $\left(K_{sp}/K_{\tau}\right)$ *is increased from 0.25 to 0.5 to 1, the microtubule stress is seen to increase due to increased load transfer by stiffer cross-linkers. The effect of increase of spectraplakin stiffness on the load transfer and cortical elongation are seen in the schematic insets (1) and (2). Stiffer spectraplakin restrict the elongation of the axonal cortex, while transmitting higher stresses to the MTs.*

Apart from constitutive parameters, geometrical parameters also play an essential role in regulating the load transfer mechanisms. Specifically, if there are more spectraplakin cross-linking the MT to the cortex in a unit cell, we can expect them to transfer more load to the MT collectively. We, therefore, vary the relative spectraplakin spacing $\left(d_{sp}/d_{\tau}\right)$ from 1 to 10 keeping other parameters unchanged. We expect that increasing the spectraplakin spacing reduces the number of spectraplakin cross-linker in parallel, and therefore is qualitatively equivalent to reducing the spectraplakin stiffness –typical mechanical behavior of springs in parallel. Indeed, we see that increasing the spectraplakin spacing is observed to result in a lower MT and increased cortical stress. Increasing the spectraplakin spacing, therefore, results in a reduced load transfer to the MT core, thereby shielding it against the applied load. Additionally, since an increased spectraplakin spacing results in increased cortical stress and thereby cortical elongation, we can expect an increase in the axonal elongation as well. Interestingly, we note that the spectraplakin elongation, $(u_s - u_1)$, also increases with an increase in spectraplakin spacing, thus increasing the load being transferred by individual cross-linker proteins. However, since the number of spectraplakin linkers has decreased, the total stress transferred from the cortex to the MT core reduces.

Role of Spectraplakin Viscosity

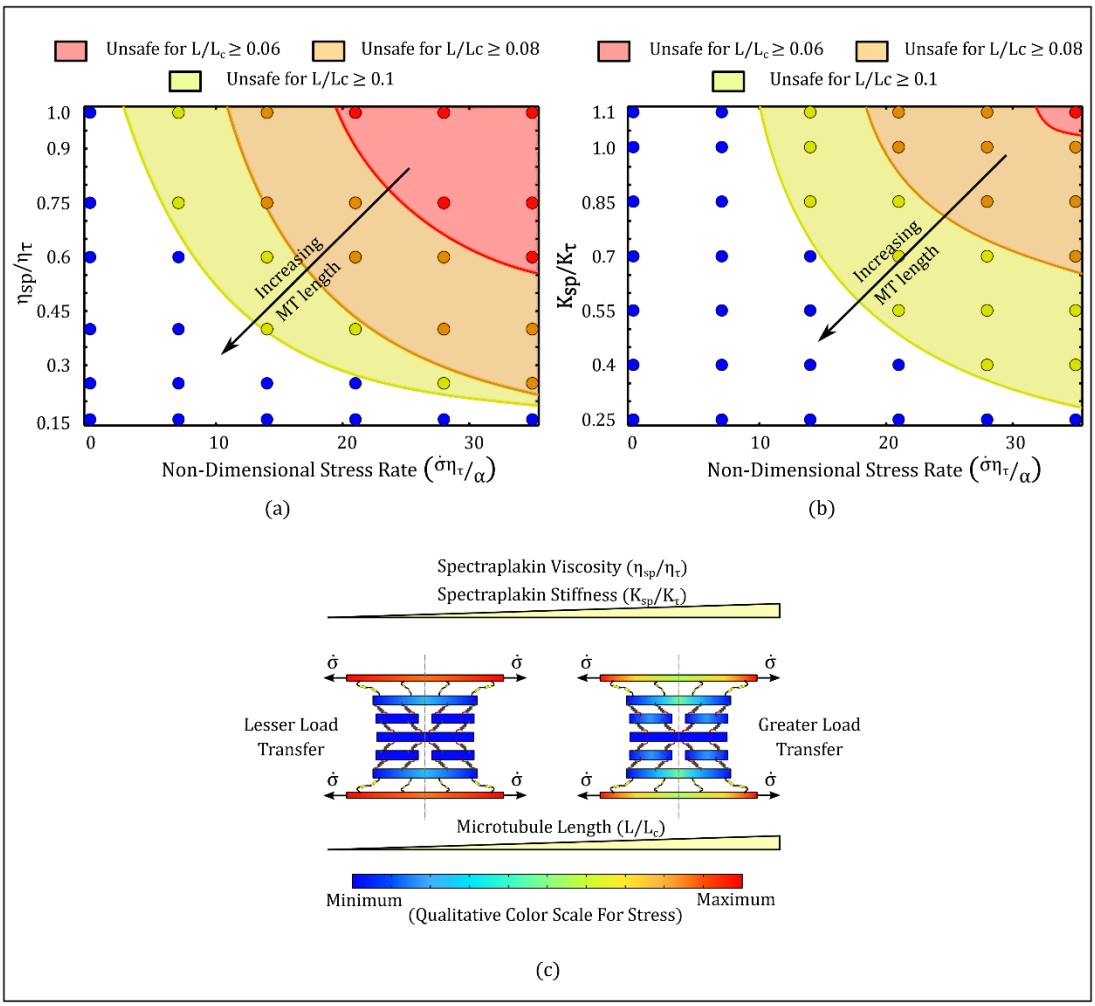

Fig S3: *Phase diagrams illustrating the safe/unsafe parameter space for spectraplakin parameters (a) Non-dimensional spectraplakin viscosity* (η_{sp}/η_{τ})*, and (b) Non-dimensional spectraplakin stiffness* (K_{sp}/K_{τ}) *at various non-dimensional stress rates* $(\dot{\sigma}\eta_{\tau}/\sigma_{max})$*. The diagrams incorporate the microtubule length* L *dependence as well. Blue dots denote a safe parameter space with no microtubule breaking. Yellow region denotes the parameters space in which the microtubules longer than* $2 \times 0.1 \times L_c$ *will fail. Orange region denotes the parameters space in which the microtubules longer than* $2 \times 0.08 \times L_c$ *will fail. Red region denotes the parameters space in which the microtubules longer than* $2 \times 0.05 \times L_c$ *will fail. In general, more dynamic loading at higher spectraplakin stiffness or viscosity. The direction of the arrows in the plot indicates that longer microtubules result in larger unsafe parameter space. (c) A schematic to depict the effects of the spectraplakin viscosity and stiffness, and microtubule length on the load transfer in the cytoskeletal unit cell.*

At a given tissue stress rate increasing the viscosity of cross-linkers effectually increases their stiffness, resulting in a higher load transfer to the MT's, thereby increasing their susceptibility to failure. A convenient means for capturing the joint effect of two parameters – the relative spectraplakin viscosity (η_{sp}/η_{τ}) and the normalized rate of applied stress $(\dot{\sigma}\eta_{\tau}/\alpha)$ – simultaneously is to create a parametric phase diagram. A phase diagram allows us to demarcate the parametric regime where the MT lattice is safe and the regime where a rupture in the MT lattice can be expected. Further, we can use the phase diagram to introduce the effects of a third parameter and observe the evolution of the unsafe parametric space as the third parameter is perturbed. Figure

S3(a) shows the combined dependence of the relative spectraplakin viscosity (η_{sp}/η_τ) and the normalized rate of applied stress $(\dot{\sigma}\eta_\tau/\alpha)$ in a phase diagram shown. In the figure, we demarcate the parameter regimes in which the MTs will survive (uncolored region) or fail (colored region) using the MT stress threshold of 7 kPa. It is immediately visible from the phase diagram (Fig S3a) that the parameter regime with higher relative spectraplakin viscosity (η_{sp}/η_τ) and higher normalized loading rate $(\dot{\sigma}\eta_\tau/\alpha)$ presents the highest risk of MT failure. Following the MT length dependence discussed previously, we see that as the normalized MT length (L/L_c) reduces from the 0.1 to 0.06, the parameter phase presenting MT failure risk shrinks from yellow to orange to red. A similar parametric dependence of the model prediction of MT stress on the parameters relative spectraplakin stiffness (K_{sp}/K_τ), the normalized rate of applied stress $(\dot{\sigma}\eta_\tau/\alpha)$ and the MT half length (L/L_c) is showed in the phase diagram in Fig S3(b).

Sensitivity Analysis

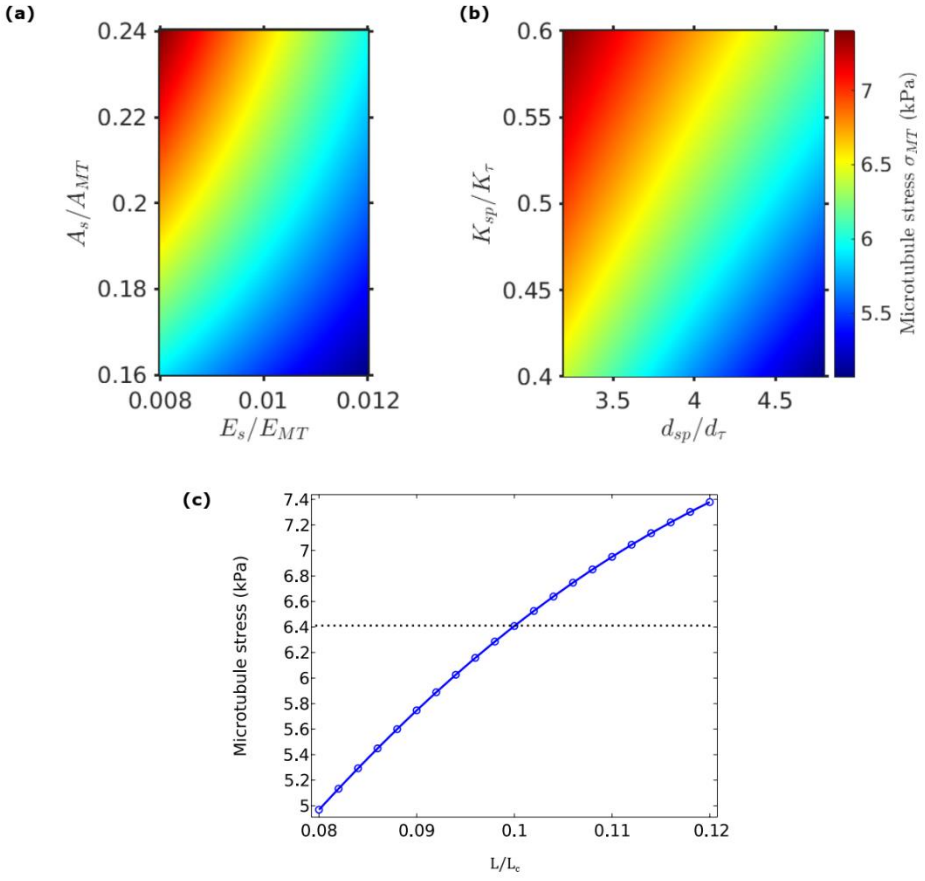

Fig S4: *Sensitivity analysis measuring the change in the model prediction of MT stress as the (a) axonal cortex parameters (elasticity v/s the cross-sectional area), (b) spectraplakin parameters (stiffness v/s distribution), and (c) the MT length vary. Each parameter is varied by* $\pm$ *20%, and in each case, we observe the predicted MT stress to vary between a range of (+17% to -22%) highlighting the importance of each of the parameters.*

Under the application of a ramped stress at a constant rate of 3 kPa/ms, leading to a tissue stress of 50 kPa, we observe how the load transferred to the MTs change as the model parameters vary. The effects of the key parameters are plotted in the form of heat map for the MT stress in Fig S4a, b. These heat maps can be useful in predicting the role of key cytoskeletal parameters, including the cortical elasticity and thickness, spectraplakin stiffness and distribution, and the MT lengths. In

Fig S4a we vary the parameters governing the mechanical behavior of the axonal cortex – the relative cortical elasticity ($0.008 < E_s/E_{MT} < 0.012$) and the relative cortical cross-sectional area ($0.16 < A_s/A_{MT} < 0.24$). It is observed that the load transferred to the MTs increases as the cortex becomes softer or thicker. Similarly, in Fig S4b we vary the parameters governing the mechanical behavior of the spectraplakin linker proteins – the relative stiffness ($0.4 < K_{sp}/K_\tau < 0.6$) and the normalized distance between consecutive spectraplakin ($3.2 < d_{sp}/d_\tau < 4.8$). We observe that the load transferred to the MTs increases as the spectraplakin linkers become stiffer or increase in number. Lastly to observe the effect of MT lengths, in Fig S4c we plot the MT stress as the MT lengths are varied ($0.08 < L/L_c < 0.12$). As the MT lengths increase more load is transferred from the tissues to the MTs. This analysis shows the role played by each parameter – allowing us to predict the physiological effects of secondary injuries which may result in chemo-mechanical alterations in the parameter values. The analysis also highlights the importance of each parameter. Absence of any of these parameters will significantly affect the model predictions.

S.5 Additional Figures

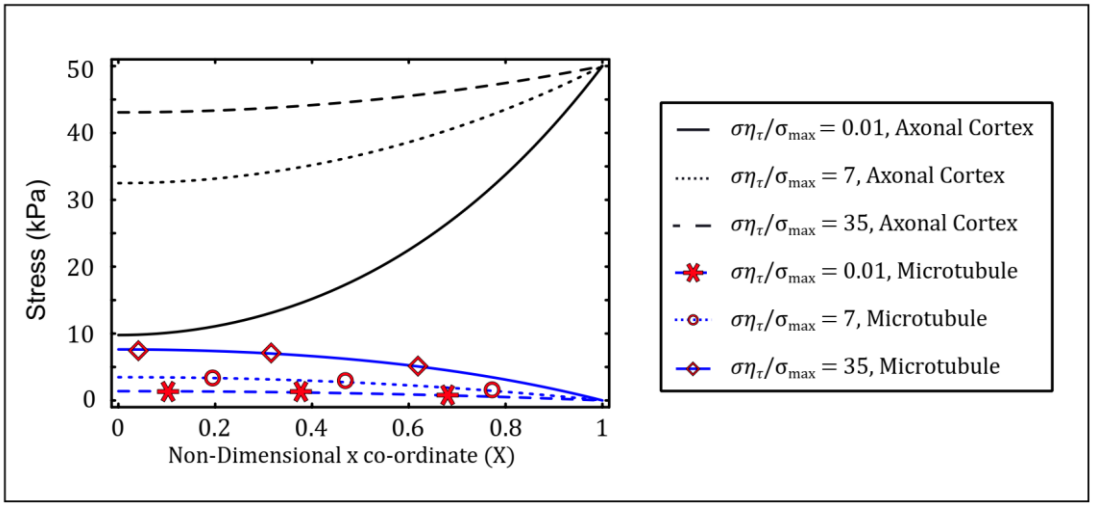

Fig S5: *The effect of changing the tissue loading rate. As the non-dimensional stress rate* ($\dot{\sigma}\eta_\tau/\sigma_{max}$) *increases from a quasi-static loading condition* ($\dot{\sigma}\eta_\tau/\sigma_{max} = 0.01$, $\dot{\sigma}$ *= 1 kPa/ms, dashed line) to a high strain rate loading condition* ($\dot{\sigma}\eta_\tau/\sigma_{max} = 35$, $\dot{\sigma}$ *= 5 kPa/ms, solid line) the stress in the axonal cortex (in black) decreases while that in the MTs (in blue) increases. So, as the tissue stress rate increases, an increased transfer of load occurs from the tissue to the MT lattice via the axonal cortex.*

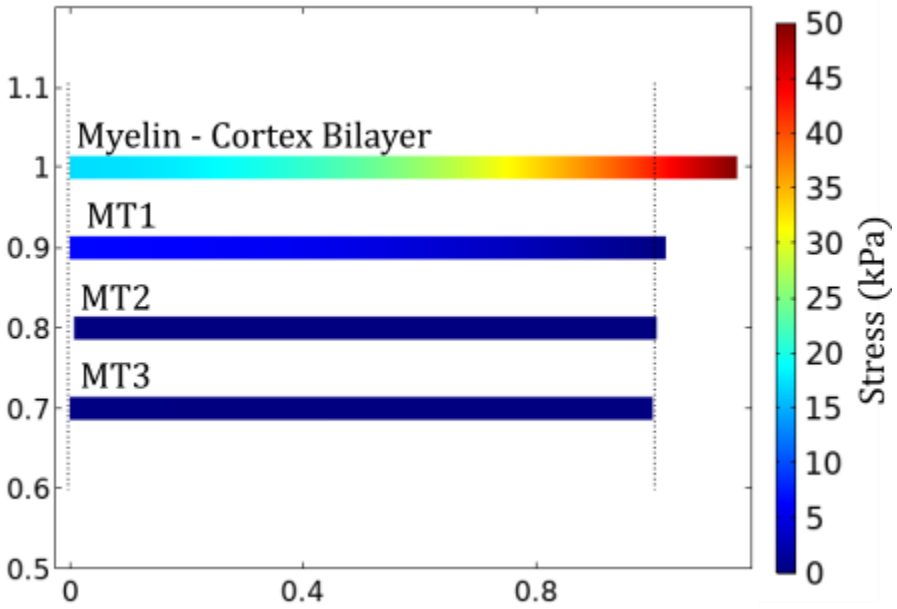

Fig S6: *A quantitatively accurate figure equivalent to the schematics of the cortical and microtubule elongation after the application of stress. On the x-axis zero is the position of the center of the unit cell where we apply the symmetry boundary condition. The elongations of the bilayer and MTs can be seen as the shifts from the dotted lines. For clarity, the cortical elongation is magnified by 100 times, while the MT elongation is magnified 10^4 times. The color in the figure quantitatively scales with the mechanical stress following the color-bar on the right. The dotted lines show the original half unit-cell of the axon. The parameter values used for this simulation are as listed in Table S1.*

References

[1] H. Ahmadzadeh, D. H. Smith and V. B. Shenoy, "Viscoelasticity of tau proteins leads to strain rate-dependent breaking of microtubules during axonal stretch injury: predictions from a mathematical model," *Biophysical journal,* vol. 106, p. 1123–1133, 2014.

[2] D. G. Siedler, M. I. Chuah, M. T. Kirkcaldie, J. C. Vickers and A. E. King, "Diffuse axonal injury in brain trauma: insights from alterations in neurofilaments," *Frontiers in cellular neuroscience,* vol. 8, p. 429, 2014.

[3] J. A. Perge, J. E. Niven, E. Mugnaini, V. Balasubramanian and P. Sterling, "Why do axons differ in caliber?," *Journal of Neuroscience,* vol. 32, no. 2, pp. 626 - 638, 2012.

[4] A. Prokop, "Cytoskeletal organization of axons in vertebrates and invertebrates," *Journal of Cell Biology,* vol. 219, 2020.

[5] S. Suresh, "Biomechanics and biophysics of cancer cells," *Acta biomaterialia,* vol. 3, p. 413–438, 2007.

[6] W. Yu and P. W. Baas, "Changes in microtubule number and length during axon differentiation," *Journal of Neuroscience,* vol. 14, p. 2818–2829, 1994.

[7] M. C. Holley and J. F. Ashmore, "Spectrin, actin and the structure of the cortical lattice in mammalian cochlear outer hair cells," *Journal of Cell Science,* vol. 96, p. 283–291, 1990.

[8] R. H. Quarles, "Myelin-associated glycoprotein (MAG): past, present and beyond," *Journal of neurochemistry,* vol. 100, no. 6, pp. 1431 - 1448, 2007.

[9] N. Snaidero and M. Simons, "The logistics of myelin biogenesis in the central nervous system," *Glia,* vol. 65, no. 7, pp. 1021 - 1031, 2017.

[10] D. F. Meaney, D. H. Smith, D. I. Shreiber, A. C. Bain, R. T. Miller, D. T. Ross and T. A. Gennarelli, "Biomechanical analysis of experimental diffuse axonal injury," *Journal of neurotrauma,* vol. 12, no. 4, pp. 689 - 694, 1995.

[11] D. H. Smith, X. H. Chen, B. N. Xu, T. K. McIntosh, T. A. Gennarelli and D. E. Meaney, "Characterization of diffuse axonal pathology and selective hippocampal damage following inertial brain trauma in the pig," *Journal of Neuropathology & Experimental Neurology,* vol. 56, no. 7, pp. 822 - 834, 1997.

[12] V. E. Johnson, W. Stewart, M. T. Weber, D. K. Cullen, R. Siman and D. H. Smith, "SNTF immunostaining reveals previously undetected axonal pathology in traumatic brain injury," *Acta neuropathologica,* vol. 131, no. 1, pp. 115 - 135, 2015.

[13] V. E. Johnson, M. T. Weber, R. Xiao, D. K. Cullen, D. F. Meaney, W. Stewart and D. H. & Smith, "Mechanical disruption of the blood-brain barrier following experimental concussion," *Acta neuropathologica,* vol. 135, no. 5, pp. 711 - 726, 2018.

[14] A. H. S. Holbourn, "Mechanics of head injuries," *The Lancet,* vol. 242, no. 6267, pp. 438-441, 1943.

[15] S. S. Margulies, L. E. Thibault and T. A. Gennarelli, "Physical model simulations of brain injury in the primate," *Journal of biomechanics,* vol. 23, no. 8, pp. 823 - 836, 1990.

[16] M. Krieg, J. Stühmer, J. G. Cueva, R. Fetter, K. Spilker, D. Cremers, K. Shen, A. R. Dunn and M. B. Goodman, "Genetic defects in β-spectrin and tau sensitize C. elegans axons to movement-induced damage via torque-tension coupling," *Elife,* vol. 6, p. e20172, 2017.